Stereochemical Effects During $[M - H]^-$ Dissociations of Epimeric 11-OH-17β-Estradiols and Distant Electronic Effects of Substituents at $C_{(11)}$ Position on Gas Phase Acidity

Sandrine Bourgoin-Voillard,[a,c] Emilie-Laure Zins,[d] Françoise Fournier,[a] Yves Jacquot,[b] Carlos Afonso,[a] Claude Pèpe,[d] Guy Leclercq,[c] and Jean-Claude Tabet[a]

[a] Université Pierre et Marie Curie, UMR 7201, Paris, France
[b] Université Pierre et Marie Curie et Ecole Normale Supérieure, UMR 7203, Paris, France
[c] Laboratoire JC Heuson de Cancérologie Mammaire, Institut Jules Bordet, Brussels, Belgium
[d] Université Pierre et Marie Curie, UMR 7075, Paris, France

The affinity of estradiol derivatives for the estrogen receptor (ER) depends strongly on nature and stereochemistry of substituents in $C_{(11)}$ position of the 17β-estradiol (**I**). In this work, the stereochemistry effects of the 11α-OH-17β-estradiol (**III**$_{\alpha}$) and 11β-OH-17β-estradiol (**III**$_{\beta}$) were investigated using CID experiments and gas-phase acidity (ΔH°_{acid}) determination. The CID experiments showed that the steroids decompose via different pathways involving competitive dissociations with rate constants depending upon the α/β $C_{(11)}$ stereochemistry. It was shown that the fragmentations of both deprotonated [**III**$_{\alpha}$-H]$^-$ and [**III**$_{\beta}$-H]$^-$ epimers were initiated by the deprotonation of the most acidic site, i.e. the phenolic hydroxyl at $C_{(3)}$. This view was confirmed by H/D exchange and double resonance experiments. Furthermore, the ΔH°_{acid} of both epimers (**III**$_{\alpha}$ and **III**$_{\beta}$), 17β-estradiol (**I**), and 17-desoxyestradiol (**II**) was determined using the extended Cooks' kinetic method. The resulting values allowed us to classify steroids as a function of their gas-phase acidity as follows: (**III**$_{\beta}$) $\gg$ (**II**) $>$ (**I**) $>$ (**III**$_{\alpha}$). Interestingly, the α/β $C_{(11)}$ stereochemistry appeared to influence strongly the gas-phase acidity. This phenomenon could be explained through stereospecific proton interaction with π-orbital cloud of A ring, which was confirmed by theoretical calculation. (J Am Soc Mass Spectrom 2009, 20, 2318–2333) © 2009 Published by Elsevier Inc. on behalf of American Society for Mass Spectrometry

The endogenous female steroid hormone 17β-estradiol (Compound **I**, E_2, Scheme **1b**) is known to play a key role in many physiologic functions of premenopausal women. Furthermore, it protects from bone loss [1] as well as cardiovascular [2] and neurodegenerative [3] diseases. Such effects result from various interactions of the hormone with the estrogen receptor (ER) [4]. The E_2/ERα complex is stabilized by hydrogen contacts occurring between, on the one hand, the hydroxyl group of phenolic A ring (E_2) and Glu-353 as well as Arg-394 of the hormone binding pocket (HBP), and on the other hand, between the 17β-hydroxyl of D-ring and His-524 (Scheme **1a**) [5–7]. Moreover, position around the functionalized site at the $C_{(11)}$ position (C ring) seems to contribute to the anchorage of the hormone within this pocket of the receptor [7–13], suggesting that steric effects at this position are important for binding affinity. Accordingly, we may consider that the proton donor character efficiency could be reinforced through electrostatic effects mediated by the nature and the stereochemistry of substituent in position 11 [14].

Mass spectrometry is widely used to characterize diastereoisomeric compound through stereochemical effects [15, 16]. Many reviews have described stereochemistry differentiation of the hydroxyl group in gas phase on rigid rings [17–22]. The stereochemical effects could provide evidence that the chemical pathways for ion-molecule reaction as well as the dissociation mechanisms promoted by negative charge from stereoisomeric ion species prepared in chemical ionization and electrospray [23]. For instance, the differentiation of alkoxides of *trans* and *cis*-cyclohexanediols has been widely described in negative chemical ionization [24–26]. This technique turned out to be also appropriate to distinguish more complex polycyclic molecules, such as mono- or polyhydroxyl norborneols, saccharides, and steroids [27–30]. The origin of stereochemical effects in these systems has been described in terms of ring strain, steric, like hyperconjugation and stereoelectronic effects due to neighboring sites of leaving group, which can

Address reprint requests to Professor J.-C. Tabet, case courrier 45, 4 place Jussieu, 75005 Paris, France. E-mail: jean-claude.tabet@upmc.fr

1044-0305/09/$32.00
doi:10.1016/j.jasms.2009.08.017

Published online September 3, 2009
Received June 19, 2009
Revised August 21, 2009
Accepted August 21, 2009

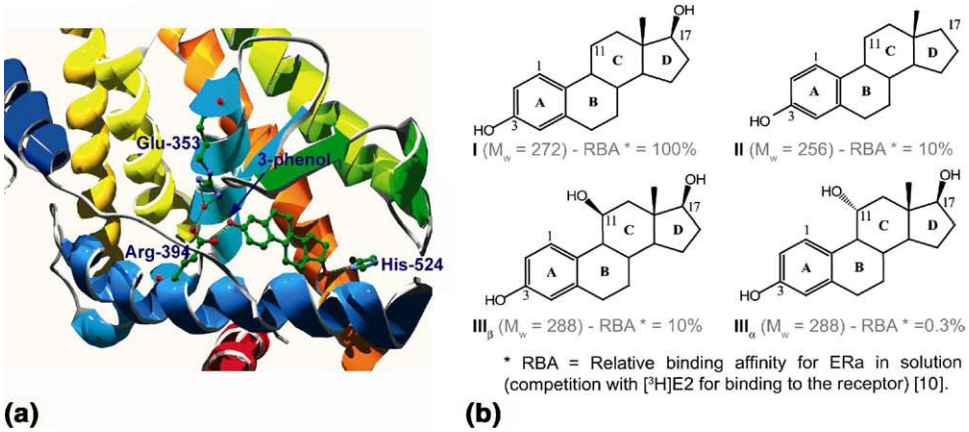

Scheme 1. (**a**) Stabilizing interactions in the human E_2/ER complex from 1ERE.PDB data using Swiss_Pdbviewer 3.7 and rendered with Pov-Ray 3.6 (H atoms are not shown). (**b**) Structures of the analytes. E_2 (**I**), 17-desoxy-E_2 (**II**), 11β-OH-E_2 (**III$_\beta$**), and 11α-OH-E_2 (**III$_\alpha$**).

involve stereospecific hydride or/and proton transfers [31]. Finally, Cooks' kinetic method [32–34] was used for such stereoisomeric distinction [35], in particular for the *cis-trans* geometry. It has been shown, for instance, that the gas-phase acidity variation of *cis-trans* methylcyclohexanol [36], 1,4-cyclohexanediols [37], and 1,2-cyclohexanediols [38] were stereochemically significant, such as 4.2 kJ mol^{-1}, 5.0 kJ mol^{-1}, and 7.1 kJ mol^{-1}, respectively. Similar differentiation has been obtained for various methyl cyclohexanols [39].

Based upon the previous consideration, the intrinsic properties of the substituted estradiol derivatives through the stereochemistry effects, for the 11α-OH-17β-estradiol (Compound **III$_\alpha$**, Scheme **1b**) and 11β-OH-17β-estradiol (Compound **III$_\beta$**, Scheme **1b**) will be investigated. To reach this aim, investigation of deprotonated phenolic site of **III$_\alpha$** and **III$_\beta$**, which is the most acidic in the studied steroids, has been considered. Indeed, the acidity values of phenolic and hydroxylic sites (secondary alcohols at $C_{(11)}$ and at $C_{(17)}$ positions) are very different, such as ~1460 kJ mol^{-1} and ~1570 kJ mol^{-1}, respectively [40].

For our work to be conclusive, we investigated gas-phase properties of the steroids (Scheme **1b**) [10]. The gas-phase acidity (ΔH°_{acid}) was evaluated by mass spectrometry using the extended Cook's kinetic method [32–34]. We were interested particularly in the stereoisomeric species through CID experiments. By this way, differences in gas-phase stability, fragmentation pathways, and gas-phase acidity were observed.

Method

The gas-phase acidity (ΔH°_{acid}) associated with a compound is typically measured using Cooks' kinetic method [32, 33] extended by Fenselau [34] and following mathematical treatment proposed by Armentrout (alternative method) [41]. This method, highly sensitive, consists of determining, in a first stage, the ratio of the k_i and k_0 rate constants associated with the competitive dissociations of a selected $[A_0 + A_i - H]^-$ deprotonated heterodimer (eqs 1a and b), where A_0 is the analyte and A_i, a reference of the known ΔH°_{acid} value.

$$[A_0, (A_i - H)]^- \xrightarrow{k_i} A_0 + [A_i - H]^- \quad (1a)$$

$$\uparrow\downarrow$$

$$[A_i, (A_0 - H)]^- \xrightarrow{k_0} A_i + [A_0 - H]^- \quad (1b)$$

$$\ln\left(\frac{I[A_i - H]^-}{I[A_0 - H]^-}\right)_{T_{eff}} \approx \ln\left(\frac{k_i}{k_0}\right)_{T_{eff}} \approx -\frac{\Delta H^\circ_{acid}(A_i)}{RT_{eff}} + \frac{GA^{app}_{T_{eff}}(A_0, A_i)}{RT_{eff}} \quad (2)$$

This approach is based on the eq 2 with $GA^{app}_{T_{eff}}(A_0, A_i) = \Delta H^\circ_{acid}(A_0) - T_{eff}\Delta\Delta S^\circ_{acid}(A_0, A_i)$ (T_{eff}: effective temperature in K [42–44]; R: Boltzmann constant ~ 8.31 J mol^{-1} K^{-1}, and $GA^{app}_{T_{eff}}$: apparent gas-phase acidity in kJ mol^{-1} [45]. In this regard, it should be noted that the A_i references require similar chemical and physicochemical properties with each other and a $\Delta H^\circ_{acid}(A_i) \sim [\Delta H^\circ_{acid}(A_0) \pm 10]$ kJ mol^{-1} [44]. Under these experimental conditions and in the used energy range, the $\Delta\Delta S^\circ_{acid}$ value is considered as constant and the plot of $\ln(k_i/k_0)$ versus $\Delta H^\circ_{acid}(A_i)$ yields a linear dependence. The slope and the x-intercept of this curve are $-1/RT_{eff}$ and $GA^{app}_{T_{eff}}$, respectively. In the case of the extended method, this experiment is performed under variable CID conditions allowing to change the effective temperature (fictitious value, which describes the behavior of ions dissociating in the time window of analyzer with non-thermal internal energy distribution) [42–44]. Finally, the relation of $GA^{app}_{T_{eff}}$ versus T_{eff} yields a linear dependence that allows an estimation of $\Delta H^\circ_{acid}(A_0)$ and $-\Delta\Delta S°(A_0, A_i)$ corresponding to the y-intercept and the slope, respectively. It should be noted that the

$\ln(k_i/k_0)$ versus $\Delta H°_{acid}(A_i)$ curves obtained using various activation amplitude conditions present a common crossing point called pseudo iso equilibriumpoint (PIP) [41] and its abscissa corresponds to $\Delta H°_{acid}(A_0)$.

First, Drahos and Vekey [46] proposed, based upon simulations, that the effective temperature range can be extended by using different analyzers, allowing to increase the proton affinity value accuracy. It is well established that the effective temperature depends on the amplitude degree of excitation, the time-scale window of the dissociation processes, and a number of other parameters [43, 44]. The measurements of proline basicity, performed by our group [47], underline the advantage of the combination of experimental results obtained with an ion trap and triple quadrupole instruments. Therefore, experiments are performed with both the ion trap and triple quadrupole instruments [47].

Experimental errors (standard deviations) were calculated from experimental deviations and taking into account uncertainties of the reference acidity values based on the Armentrout treatment [41]. More recently, Armentrout considered that errors in the $\Delta H°$ values are about ± 4 to ± 12 kJ mol^{-1} (± 9 to ± 30 J mol^{-1} K^{-1} for activation entropy differences) [73], whereas Drahos and Vekey suggested an estimated error of ± 5 kJ mol^{-1} [± 10 J mol^{-1} K^{-1} for $\Delta\Delta S°(A_0,A_i)$] [48]. In this work, the errors on $\Delta H°$ values and $\Delta\Delta S°$ values are considered to be 10 kJ mol^{-1} and 20 J mol^{-1} K^{-1}, respectively, and in addition, experimental relative deviations are provided under brackets (Table 6).

Experimental

Chemicals and Sample Preparation

Estrogenic compounds 17β-estradiol (**I**), 17-desoxyestradiol (**II**), 11β-OH-17β-estradiol (**III$_\beta$**), and 11α-OH-17β-estradiol (**III$_\alpha$**) were purchased from Steraloids Inc. (Newport, RI, USA). Methanol, triethylamine (TEA), carboxylic acids, and phenols were obtained from Sigma-Aldrich (Saint-Quentin Fallavier, France). All compounds were used without further purification. For the MS investigations (i.e., the dissociation of deprotonated stereoisomers and the gas-phase acidity determination) two different solutions were respectively used (1) for experiments performed from both ion trap and hybrid Qh/FT-ICR mass spectrometers, each compound was diluted in methanol at 30 μM with 0.4% NH_4OH to improve the formation of deprotonated species in the ESI source, and (2) steroid samples were separately dissolved in methanol, and were separately mixed at a 1:1 ratio with the appropriate acid reference (final concentrations: 70 μM and 30 μM for experiments performed by the triple quadrupole and the ion trap, respectively).

Mass Spectrometry

Experiments were performed with a triple quadrupole (Quattro I; Micromass, Manchester, UK), a 3D quadrupole ion trap (Esquire 3000; Bruker, Bremen, Germany) and a hybrid Qh/FT-ICR (ApexQe equipped with a 7 T superconducting magnet; Bruker). These instruments were equipped with ESI source operated in the negative ion mode. The used source conditions for each mass spectrometer are presented in Table 1. The conditions used to generate product ion spectra with various activation modes are described below.

Triple quadrupole mass spectrometer. For gas-phase acidity measurements, CID experiments were performed by "in axis" of ion beam activation in collision cell using argon as target gas (5.10^{-5} mBar). The laboratory frame kinetic energy was varied by voltage increase from 2 to 20 V by 2 V steps, and from 20 to 60 V by 5 V steps.

Ion trap mass spectrometer. CID experiments were carried out using resonant excitation with an excitation cutoff [49] of 20% of the *m/z* value of the precursor ion for deprotonated heterodimers (in Cooks' kinetic method experiments) and to 41% for the deprotonated steroids dissociation for mechanistic investigation.

Hybrid Qh/FT-ICR mass spectrometer. Product ion spectra using hybrid Qh/FT-ICR spectrometer were obtained from different activation modes. First, CID experiments within non-resonant conditions were carried out in the hexapole linear ion trap used for ion storage

Table 1. Experimental conditions for ESI mass spectra

	Analyzer	Sample flow (μL/h)	T (°C)	Drying gas flow (L/h)	Nebulizer (psi)	Capillary potential (V)	Orifice-skimmer offset ΔV (V)
Gas phase acidities	Triple quadrupole	400	80	250	20 (L/h)	−3000	−16[a], −13[b], −18[c], −15[d]
	Ion trap	140	190	180	3	+3000	−20[a], −16[b], −44[c], −30[d]
Stereoisomer	Ion trap	140	200	300	6	+3000	−63
Distinction	Qh/FT-ICR	140	250	180	22	+4500	−20*

[a] for **I**.
[b] for **II**.
[c] for **III$_\beta$**.
[d] for **III$_\alpha$**.
* ΔV(skim 1-ion funnel 2) and IF1 = −150 V, IF2 = −10 V.

as well as for collisional ion activation. The laboratory frame kinetic energy (E_{lab}) was set to 20 V for estradiol epimers. As expected, this activation mode led to product ions similar to those obtained in the quadrupole ion trap instrument.

Second, SORI-CID experiments (with −1800 Hz frequency offset) performed in the ICR cell yielded only a few low abundance product ions. This behavior contrasts with results obtained from infrared multiphoton dissociation (IRMPD) experiments (CO_2 laser) giving rise to product ions formation similar to those obtained in the CID spectra performed in the hexapole collision cell. Hence, in the present work, only results obtained under CID (in the hexapole collision cell) and IRMPD are presented.

Moreover, double resonance (DR) experiments were performed for both the **III**$_\alpha$ and **III**$_\beta$ stereoisomers. Typically, the precursor ion was irradiated with the IR laser and simultaneously one product ion was continuously ejected at different voltage values (from 0 to 20 V) by applying a dephased rf dipolar potential (10–20 $V_{p\text{-}p}$) at excitation plates of the ICR cell. These experiments were carried out using a modified pulse program with Xmass software (Bruker).

Theory

DFT calculations were performed using the Gaussian 03 software [50]. All structures were optimized using the Becke exchange functional (B) [51], with three hybrid parameters along with the Perdew (P86) non-local correlation functional correlation [52, 53]. Full optimizations were performed at the B3P86/6-31+G* level of calculation [54, 55]. Frequency calculations were carried out at the same level of theory, to take into account the zero point energy correction (ZPE). Previous studies have shown that B3P86/6-31+G* level of calculation allowed to reproduce experimental results, such as cationic affinities, for similar compounds [56, 57].

Different structures were considered, built, and fully optimized, and some of these structures are presented in the Table 2. This table allows comparison of the stability of different conformers corresponding to both **III**$_\beta$ and **III**$_\alpha$ stereoisomers. It should be noted that some structures are not stable in the gas phase. Furthermore, several conformers are energetically close to each other, suggesting that different conformers can be formed.

Results and Discussion

In this work, we were interested in investigating the gas-phase behavior of the $C_{(11)}$ stereochemistry of hydroxyl group substituted estradiols. This position is known to yield significant modification of the E_2 (**I**) affinity for ERα in solution [7, 10–13]. In fact, it is assumed that this behavior may be relevant not only to new ligand-ER interactions generated by the substituent at the $C_{(11)}$ position, but also electronic factors capable of modulating the phenol proton mobility. In solution, direct interactions are often masked by solvent molecules, such as water. For this reason, the gas-phase, i.e., within the absence of solvent, is a good condition to study the steroid intrinsic properties, such as the gas-phase acidity and phenoxide stability, which can influence noncovalent interactions as well as the gas-phase dissociation of such reagents.

Distinction of the **III**$_\alpha$ *and* **III**$_\beta$ *Stereoisomers*

Investigation of the fragmentation of estradiol derivatives, in particular the study of stereochemistry effects on both isomers 11αOH-E_2 (**III**$_\alpha$) and 11βOH-E_2 (**III**$_\beta$), could be of interest to identify the role of hydroxyl deprotonation at $C_{(11)}$. In this work, differences in the stability and fragmentations as a function of the stereochemistry have been observed. These results should depend on the deprotonation site, which is not necessary the hydroxyl at $C_{(11)}$. Three deprotonation sites could be envisaged: hydroxyl at $C_{(11)}$, hydroxyl at $C_{(17)}$, and the phenolic hydroxyl at $C_{(3)}$. The latter seemed the appropriate site to initiate the fragmentations because it is the most acidic site. Hence, the aim of this section was to understand the fragmentation pathways and to determine the different deprotonation sites.

CID mass spectra and ERMS investigations with ion trap. Substituted **III**$_\alpha$ and **III**$_\beta$ estradiols with a hydroxyl group located at the $C_{(11)}$ position in the α and β configurations, respectively (Scheme **1b**) should yield particular reactivity towards collisional activation, which should be very informative for enlightening electronic effects. In negative ion mode, the ESI mass spectra of the stereoisomeric substituted estradiols recorded using the ion trap instrument are characterized by an abundant $[M - H]^-$ ion (*m/z* 287) without any "in source" fragmentation. From their CID spectra, their stereochemical distinction is poor since under standard resonant excitation conditions (i.e., with automated LMCO calculation, 77 Th), the activated precursor ions are ejected from the ion trap cell before formation of product ions. This behavior results from the depth of the Dehmelt pseudo-potential well, which is not deep enough compared with the kinetic energy required for reaching the $[M - H]^-$ ion dissociation threshold. Consequently, the increase of the ion excitation low mass cutoff, e.g., at 120 Th (i.e., $q_{z(exc)} = 0.379$), allows to reach more efficient resonant excitation from precursor ion storage within a deeper Dehmelt pseudo-potential well in the stability diagram [49]. Under these q_z isolation/excitation conditions, higher amplitude of the AC excitation can be applied without premature precursor ion ejection. It results in the enhancement of product ions in abundance and variety. The CID spectra present a rich profile of product ions characterizing the dissociation of polycyclic systems [58, 59]. Therefore, the CID spectra (Figure 1) of the deprotonated $[\mathbf{III}_\alpha\text{-H}]^-$ and $[\mathbf{III}_\beta\text{-H}]^-$ epimers display significant stereochemi-

Table 2. Influence of the conformation on the relative stability of the neutral compounds

Stereoisomer	Structure	Energy (Hartree)	ΔE (kJ mol^{-1})
III$_\alpha$	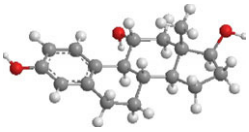	−928.48411	0.0
	III$_\alpha$-1 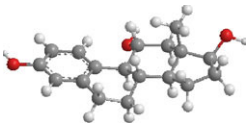	−928.48403	0.2
	III$_\alpha$-2 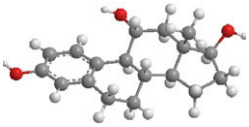	−928.48159	6.6
	III$_\alpha$-3 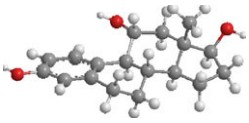	Not stable: collapse to structure **III**$_\alpha$-1	
III$_\beta$	**III**$_\alpha$-4 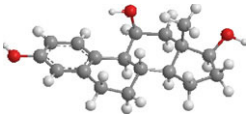	−928.48560	0.0
	III$_\beta$-1 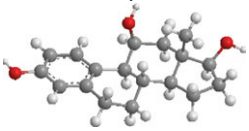	−928.48226	8.8
	III$_\beta$-2 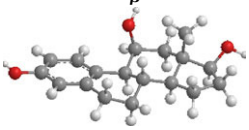	Not stable: collapse to structure **III**$_\beta$-2	
	III$_\beta$-3 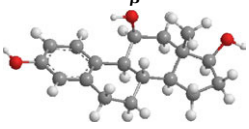	Not stable: collapse to structure **III**$_\beta$-1	
	III$_\beta$-4		

ΔE = $E_{considered\ structure} - E_{of\ the\ most\ stable\ structure}$.

cal effects resulting into a relative abundance variation of the survival precursor ions (i.e., *m/z* 287) and the product *m/z* 285, 269, 259, and 257 ions. The respective formation of the latter series as diagnostic ions involves small mass neutral releases, which will be discussed later.

To improve stereoisomer differentiation in terms of ion abundance variation, energy-resolved mass spectra (ERMS) experiments [60] were performed by raising the resonant excitation amplitude from 1.00 to 1.55 $V_{p\text{-}p}$ (Figure 2). This differentiation is based upon both the precursor and product ion relative abundance evolutions.

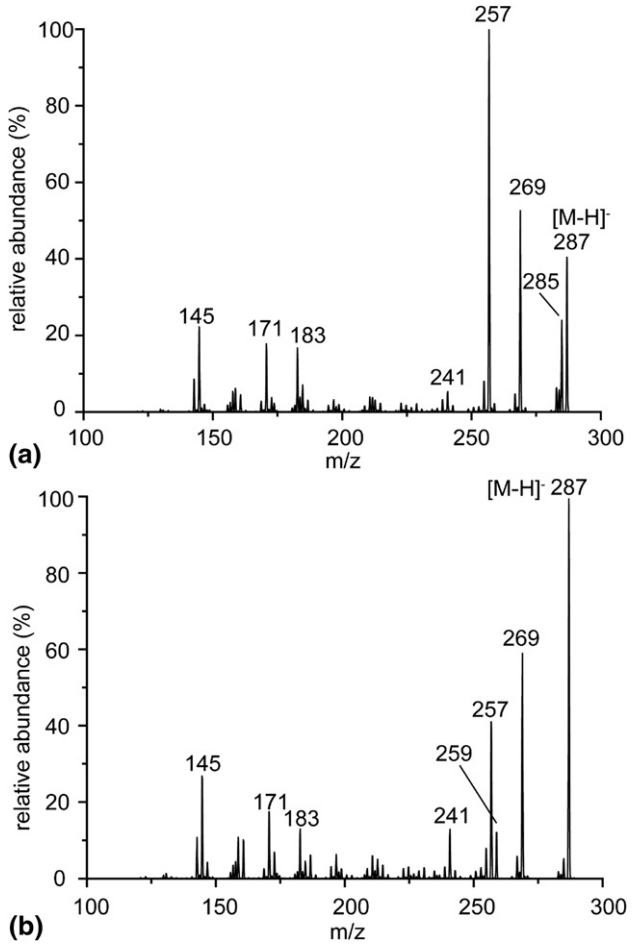

Figure 1. CID spectra of (**a**) 11α-OH-17β-E_2, $\mathbf{III}_{\boldsymbol{\alpha}}$, (**b**) 11β-OH-17β-$E_2$, $\mathbf{III}_{\boldsymbol{\beta}}$ recorded by excitation amplitude at 1.40 $V_{p\text{-}p}$ using quadrupole ion trap.

From the breakdown curve evolution of the precursor ions, different behaviors can be shown as a function of the considered estradiol epimers:

- the $V_{1/2}$ value (corresponding to the excitation voltage amplitude required for decomposition of half of the precursor ion population) increases from 1.31 ± 0.05 $V_{p\text{-}p}$ to 1.38 ± 0.05 $V_{p\text{-}p}$ for $[\mathbf{III}_{\boldsymbol{\alpha}}\text{-H}]^-$ and $[\mathbf{III}_{\boldsymbol{\beta}}\text{-H}]^-$, respectively;
- the decay (at low-energy) of $[\mathbf{III}_{\boldsymbol{\beta}}\text{-H}]^-$ precursor ion is more pronounced than that of the $[\mathbf{III}_{\boldsymbol{\alpha}}\text{-H}]^-$ ion and thus, the linear part of slope around the $V_{1/2}$ values of the $[\mathbf{III}_{\boldsymbol{\beta}}\text{-H}]^-$ dissociation curve is more abrupt.

Both, the latter parameters (i.e., curvature at the beginning and slope at $V_{1/2}$) reflect different properties of transition-state (i.e., loose over tight configuration) as well as entropic effects [61, 62]. It results from these effects a $V_{1/2}$ shift toward the higher energy range.

Mechanism of formation of diagnostic ions based on high-resolution measurements and labeled experiments. Different product ions are more or less favored according to the studied stereochemistry of precursor ions. Formation of the *m/z* 257 ion corresponds to the main dissociative pathway for the α epimer, whereas from the β epimer the *m/z* 269 ion becomes the base peak. Moreover, from the latter, the rate constant of the *m/z* 259 formation is significantly enhanced, whereas that of *m/z* 285 is lowered. Then, the product ion abundances reflect clearly the dependence of the dissociation rate constants upon the $C_{(11)}$ substituted estradiol stereochemistry [28] although the released groups are distant to the phenolic site favorably deprotonated as seen later.

To rationalize the fragmentation orientation, elemental composition of neutral losses should be a useful tool for such aim. The elemental composition of product ions, generated from the CID experiments (see the Experimental section) performed in the hexapole collision cell of the hybrid Qh/FT-ICR instru-

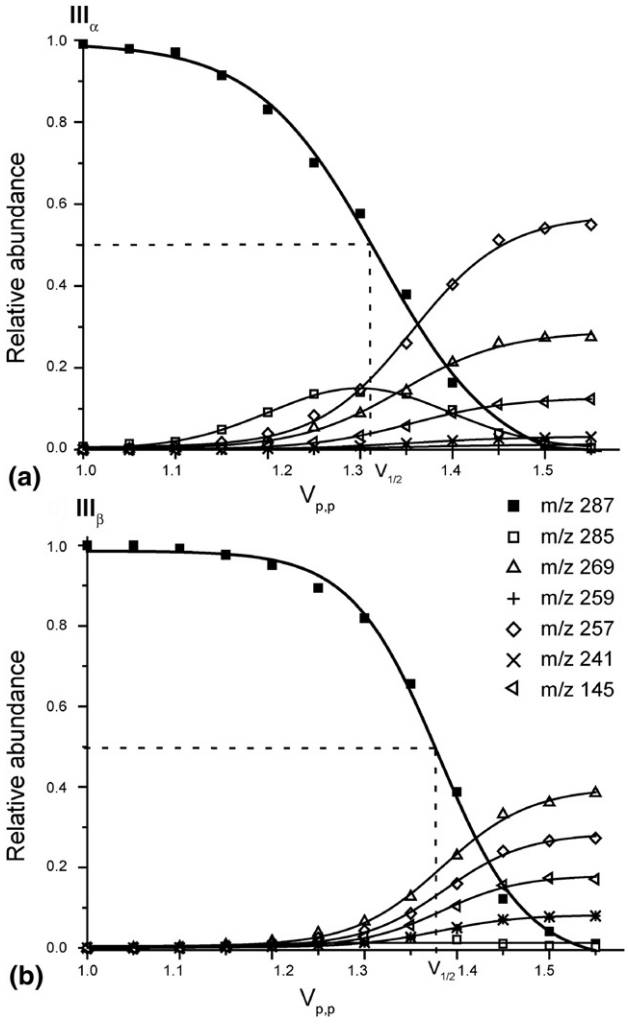

Figure 2. ERMS breakdown dependences on deprotonated ions prepared in ESI conditions from (**a**) 11α-OH-17β-E_2, $\mathbf{III}_{\boldsymbol{\alpha}}$, (**b**) 11β-OH-17β-$E_2$, $\mathbf{III}_{\boldsymbol{\beta}}$ recorded by excitation amplitude rise from 1.5 $V_{p\text{-}p}$ to 2.2 $V_{p\text{-}p}$. [(filled square) *m/z* 287, (open circle) *m/z* 269, (open square) *m/z* 259, (open triangle) *m/z* 257, (×) *m/z* 241, (open diamond) *m/z* 145].

Table 3. Very high resolution measurements of product ions of CID spectra (E_{lab} = 20 V) of the epimeric [**III**$_\alpha$-H]$^-$ (a) and [**III**$_\beta$-H]$^-$ (b) (*m/z* 287, $C_{18}H_{23}O_3$) ions in collision cell of the hybrid Qh/FT-ICR instrument

Measured *m/z* values		Relative abundance		Elemental formula	Calculated *m/z* values	Error (ppm)		Neutral loss
(a)	(b)	(a)	(b)			(a)	(b)	
287.16525	287.16541	1.000	1.000	$C_{18}H_{23}O_3$	287.16527	0.1	0.5	
285.14978	285.14989	0.193	0.017	$C_{18}H_{21}O_3$	285.14962	1.0	1.0	H_2
269.15492	269.15486	0.059	0.030	$C_{18}H_{21}O_2$	269.15470	0.8	0.6	H_2O
259.17049	259.17048	0.002	0.003	$C_{17}H_{23}O_2$	259.17035	0.5	0.5	CO
(c)	259.13403	(c)	0.004	$C_{16}H_{19}O_3$	259.13397		0.2	C_2H_4
257.15481	257.15476	0.028	0.015	$C_{17}H_{21}O_2$	257.15470	0.4	0.2	CH_2O or/and H_2 + CO
257.11843	257.11838	0.052	0.005	$C_{16}H_{17}O_3$	257.11832	0.4	0.2	C_2H_6 or/and H_2+ C_2H_4

(a) from **III**$_\alpha$, (b) from **III**$_\beta$, (c) not observed.

ment (Table 3), have been studied (note that a similar precursor ion behavior is shown under IRMPD conditions into the ICR cell). CID spectra of [M − H]$^-$ deprotonated diastereomers display more complicated profiles due to presence of isobaric product ions, especially for *m/z* 259 and 257 (Table 3). However, the product ion abundances relative to the precursor ions are significantly reduced from dissociation occurring in the hexapole activation cell of the Qh/FT-ICR instrument compared with those observed from dissociations generated in the ion trap where the LMCO value could be changed, as explained previously.

In addition to the high-resolution experiments, the cleavage specificity of the selected precursor ion was investigated from its labeling form prepared through proton/deuteron exchanges from sample solution in MeOD, which is directly introduced by pump infusion in source. The H/D exchange experiments from both the **III**$_\alpha$ and **III**$_\beta$ epimers mainly yield generation of the bis-deuterated [**III**$_{\alpha,d3}$-D]$^-$ and [**III**$_{\beta,d3}$-D]$^-$ species (*m/z* 289) (~75%) in which, very likely, the deuterium must be located at the $C_{(11)}$ and $C_{(17)}$ hydroxyl groups, as they are the less acidic sites. Under the same low-energy collision conditions, the product ion spectra of the epimeric [**III**$_{d3}$-D]$^-$ ions (*m/z* 289) mainly displayed four diagnostic product ions presenting one or more deuterium in different proportion as reported in Table 4.

m/z 285 Product Ion Due to Loss of H_2

The *m/z* 285 product ions were observed from both the deprotonated [**III**$_\alpha$-H]$^-$ and [**III**$_\beta$-H]$^-$ epimers unambiguously corresponding to H_2 release, which is significantly enhanced by the [**III**$_\alpha$-H]$^-$ epimer. From experiments performed at high or low collision energy range, this elimination characterizes usual dissociation of the primary and secondary alkoxide species [26, 63–67]. This cleavage is sensitive to the stereochemistry of the studied hydroxylic system. This elimination takes place generally when alkoxide promotes formation of hydride sterically neighboring another acidic site [66]. In this particular case, the H_2 loss is entropically favored compared with that occurring from more distant mobile proton. On the other hand, the observed stereochemical effect must reflect either a minor role of ion–dipole complex [(M − 2H), H$^-$] (i.e., the A ion-dipole complex, Scheme 2) or the occurrence of one competitive reaction (stereochemically controlled), which is favored by the [**III**$_\beta$-H]$^-$ epimer.

After selection (narrow isolation window) and collisional activation of the *m/z* 289 ions, these precursor ions lead specifically to formation of [(**M**$_{d3}$-D)-HD]$^-$ product ions (*m/z* 286), independently of the stereochemistry (Table 3).

If deprotonation occurs regioselectively at the phenolic site of the A ring, deuterium of the HD loss may be removed from labeled hydroxyl groups at $C_{(11)}$ or/and at $C_{(17)}$. To reach information on the hydrogen loss mechanism, the CID spectrum of the deprotonated 17β-estradiol [**I**-H]$^-$ (*m/z* 271) was recorded (data not shown). Apparently, this CID spectrum presents significant loss of H_2. When this experiment is repeated with the labeled form, i.e., [I_{d2}-D]$^-$ (*m/z* 272), there appears an unexpected specific H_2 loss. This behavior indicates that the benzylic hydride removing at $C_{(9)}$ position can

Table 4. Labeling of product ions produced by low energy CID experiments (resonant excitation of 1.5 $V_{p\text{-}p}$) from both [M_{d3}-D]$^-$ epimeric ions (from **III**$_\alpha$ and **III**$_\beta$) (*m/z* 289)

Product ions (labeling)	Attributed neutral losses	Abundance of product ion from the epimeric [M_{d3}-D]$^-$ precursor (±2%)	
		III$_\alpha$	**III**$_\beta$
286 (1D)	HD	100%	100%
271 (2D)	H_2O	0%	33%
270 (1D)	HDO	100%	67%
261 (2D)	C_2H_4		100%
259 (2D)	CH_2 = O	14%	60%
258 (1D)	CHD = O	21%	15%
	HD + C_2H_4	65%	25%

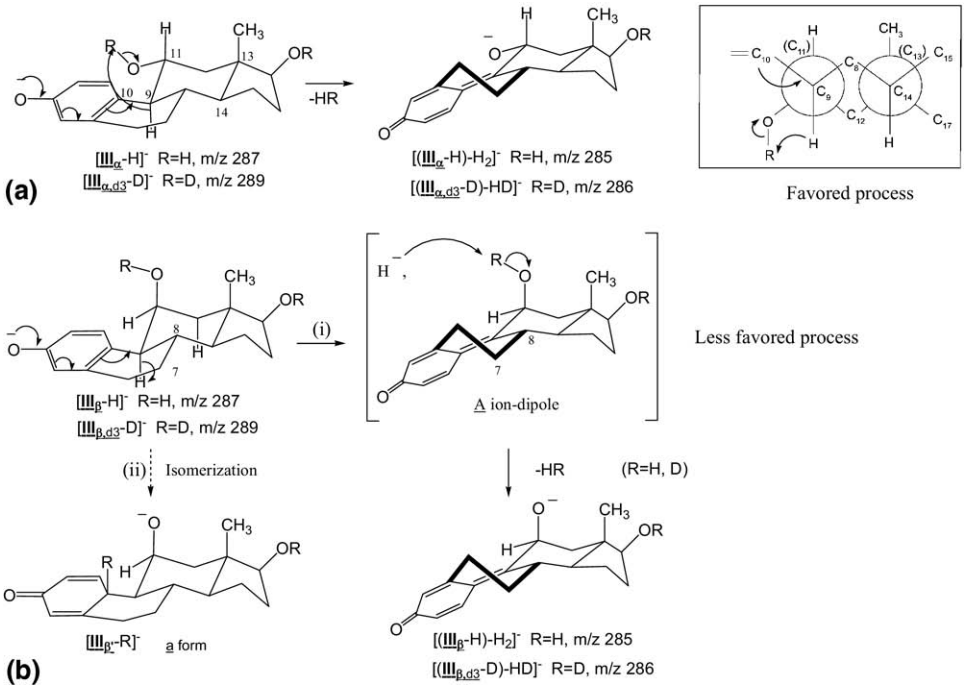

Scheme 2. Proposed structure for the deprotonated ions of (**a**) $\mathbf{III}_\alpha$ and (**b**) $\mathbf{III}_\beta$ for the loss of HD.

react with the more neighbored activated proton rather than from most acidic site, i.e., at $C_{(17)}$ position. This loss of neighboring H_2 molecule does not allow to rule out the formation of the A ion–dipole complex [(M-D-H),H^-] (Scheme **2b**). Such hydride–dipole complexes were introduced more than 20 years ago [36]. Thus, the loss of H_2 from $[\mathbf{I}_{d2}\text{-D}]^-$ (*m/z* 272) indicates that the deuterium of the OD group at $C_{(17)}$ is not involved in this process. Hence, in the case of both the α and β epimers, the loss of HD reflects the removing of D from $C_{(11)}$ rather than $C_{(17)}$. Indeed, a mobile deuteron of the hydroxylic group at $C_{(11)}$ is close to the $C_{(9)}$ hydride release site.

To rationalize the HD loss, which is enhanced for $[\mathbf{III}_{\alpha,d3}\text{-D}]^-$ compared with that observed from $[\mathbf{III}_{\beta,d3}\text{-D}]^-$, the negative charge at $C_{(3)}$ must promote the hydride transfer from the benzyl $C_{(9)}$ position to the neighbored OD group allowing the favorable HD release as shown by the Newman representation (Scheme **2a**). Such decomposition pathway is not favored by the $[\mathbf{III}_{\beta,d3}\text{-D}]^-$ epimeric ions, because of the more distant axial OD group at $C_{(11)}$ position [180° dihedral angle, Scheme **2b**(i)], which quenches the mobile proton lowering the H_2 release rate constant. In this regard, to support this interpretation, DFT calculations were performed, allowing determination of the most stable conformation (vide infra). Such stereochemical effects were described a long time ago from alicyclic compounds [36, 63–67]. The HD loss can occur through the formation of an hydride–dipole A complex although, competitively, a stereospecific isomerization [*a* form, Scheme **2b**(ii)] is more favorable.

m/z 269 Product Ion: Various Mechanisms for the Regioselective Water Loss from the $C_{(11)}$ Position

The loss of 18 u from $[M - H]^-$ could be attributed to a water release as shown from the very high-resolution measurements on the FT-ICR instrument (Table 3) rather than a possible isobaric neutral due to consecutive (H_2 + CH_4) losses. The H_2O loss is significantly the most favored decomposition pathway from the $[\mathbf{III}_\beta\text{-H}]^-$ epimeric ions (Figures 1 and 2).

The CID spectra of the labeled $[\mathbf{III}_{\alpha,d3}\text{-D}]^-$ precursor ions (*m/z* 289) display a stereospecific loss of HDO (i.e., 100%) in contrast to the β epimeric ion which gives rise to formation of the $[(\mathbf{III}_{\beta,d3}\text{-D})\text{-}H_2O]^-$ and $[(\mathbf{III}_{\beta,d3}\text{-D})\text{-HDO}]^-$ product ions (Table 4) in an abundance ratio of 33% and 67%, respectively. The stronger acidity of the phenol group allows orienting the elimination of water from the less distant hydroxyl site, i.e., at $C_{(11)}$ (a mechanism is proposed in supplementary material, S1). Indeed, it is difficult to consider water release from the $C_{(17)}$ position, which is too far from the charge in this intact polycyclic systems that involves intact rings.

m/z 259 Product Ions: C_2H_4 Loss as a Stereospecific Process

The CID experiment of the *m/z* 287 $[M - H]^-$ ion recorded using the FT-ICR instrument displays two isobaric product ions at *m/z* 259.1705 and 259.1340 corresponding, respectively, to the CO and C_2H_4 releases (Table 3). The loss of CO is not stereospecific (i.e., being observed for both the α and β epimers), whereas

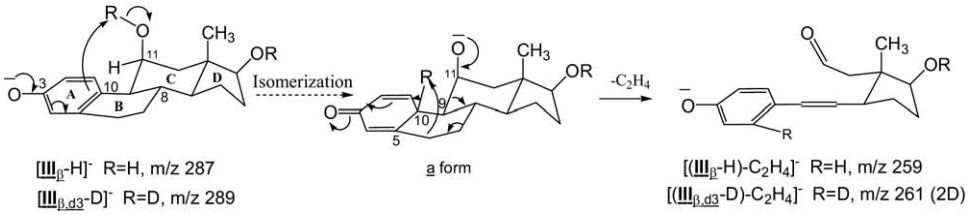

Scheme 3. Proposed structure for the deprotonated ions of $\mathbf{III}_{\boldsymbol{\beta}}$ for the loss of C_2H_4.

the loss of C_2H_4 is observed exclusively from the $[\mathbf{III}_{\boldsymbol{\beta}}\text{-H}]^-$ ion. This stereospecific release could be rationalized from dissociation of the isomerized *a* form of $[\mathbf{III}_{\boldsymbol{\beta}}\text{-H}]^-$ (Scheme 3). In competition with the proton migration used for the water loss, the 11β alkoxide *a* form (Scheme 3) can promote concomitant B/C ring cleavages leading to the C_2H_4 neutral loss. This process occurs via migration of the proton at $C_{(10)}$ to the phenylic $C_{(9)}$ site. According to this pathway, the $[(\mathbf{III}_{\boldsymbol{\beta}}\text{-H})\text{-}C_2H_4]^-$ ion appears more stable (aromatic species) than the isomerized *a* form. This proposed mechanism is consistent with the H/D exchange experiments, which indicates that both the deuterium atoms are preserved during the ethylene loss. Indeed, 100% of the *m/z* 259 is shifted to *m/z* 261 for $[\mathbf{III}_{\boldsymbol{\beta}}\text{,d3-D}]^-$ (*m/z* 289) ion dissociation. Hence, this stereospecific loss is initiated by the proton transfer for the $\mathbf{III}_{\boldsymbol{\beta}}$ epimer, whereas this release does not take place for the $\mathbf{III}_{\boldsymbol{\alpha}}$ epimer. For the latter, the hydride transfer from $C_{(9)}$ is favored, and orients toward other reactions.

m/z 257 Product Ions Favored for the α Epimer as Resulting from Consecutive (H_2+ C_2H_4) Neutral Loss

As before, from $[M - H]^-$ ions dissociation measured under very high-resolution conditions, the nominal *m/z* 257 is composed of two isobaric product ions detected at *m/z* 257.15,476 and 257.11,838 corresponding to the formal CH_2O and C_2H_6 releases, respectively (Table 3). The CH_2O loss is more intense in the case of the β epimer ion (i.e., CH_2O/C_2H_6:3/1) than with the α epimer as the $[\mathbf{III}_{\boldsymbol{\alpha}}\text{-H}]^-$ ion yields more favorably the formal C_2H_6 loss (i.e., CH_2O/C_2H_6:7/13) (Table 4).

Note that the formal CH_2O and C_2H_6 neutral losses (i.e., 30 u) can take place either directly or via consecutive neutral releases as (H_2+ CO) and (H_2+ C_2H_4). To verify this hypothesis, double resonance experiments were performed cautiously on the $[\text{M-H-H}_2]^-$ product ions (*m/z* 285) in the ICR cell during the $[\mathbf{III}_{\boldsymbol{\alpha}}\text{-H}]^-$ and $[\mathbf{III}_{\boldsymbol{\beta}}\text{-H}]^-$ precursor ion activation by IRMPD (Figure 3a_1 and b_1). The *m/z* of precursor ions being close to the *m/z* of the continuously ejected $[(\mathbf{M}\text{-H})\text{-H}_2]^-$ (*m/z* 285) product ion, the DR amplitude was increased by weak voltage steps to avoid the $[\mathbf{M}\text{-H}]^-$ precursor ion ejection (Figure 3). Figures 3a_1 and b_1 present the evolution of *m/z* 285 ion abundance as a function of the ejection amplitude, it is shown that relatively low voltages are required to eject these ions. The relative abundance of the main product ions is presented in Figures 3a_2 and b_2 for the α and β epimers, respectively. It is shown that for the α epimer, the abundance of the high mass product ions, such as *m/z* 259 and 241 (Figure 3a_2), are not affected by the $[\mathbf{III}_{\boldsymbol{\alpha}}\text{-H-H}_2]^-$ ion ejection. Most notably, the intensity of the $[(\mathbf{III}_{\boldsymbol{\alpha}}\text{-H})\text{-}(H_2 + C_2H_4)]^-$ ion (*m/z* 257) decreases significantly whereas that of the $[(\mathbf{III}_{\boldsymbol{\alpha}}\text{-H})\text{-}(H_2CO)]^-$ product ion (*m/z* 257) remains constant (Figure 3a_2). Thus, it can be considered that the *m/z* 257.11,838 ion corresponds to $[(\mathbf{III}_{\boldsymbol{\alpha}}\text{-H})\text{-}(H_2 + C_2H_4)]^-$ and is mainly produced by subsequent loss of C_2H_4 from the $[\mathbf{III}_{\boldsymbol{\alpha}}\text{-H-H}_2]^-$ ion. Note that the consecutive dissociation of $[(\mathbf{M}\text{-H})\text{-H}_2]^-$ is confirmed by the ERMS curves (Figure 2a). Indeed, its abundance rises until 1.3 $V_{p\text{-}p}$, and then decreases as consecutive decomposition takes place.

Concerning the β epimer, a similar modification of the $[\mathbf{III}_{\boldsymbol{\beta}}\text{-H}]^-$ IRMPD spectrum is observed during the controlled DR experiment performed on the $[\mathbf{III}_{\boldsymbol{\beta}}\text{-H-H}_2]^-$ product ion. Indeed, a three-time decrease of the low signal intensity of the $[(\mathbf{III}_{\boldsymbol{\beta}}\text{-H})\text{-}(H_2 + C_2H_4)]^-$ is observed in contrast with the $[(\mathbf{III}_{\boldsymbol{\beta}}\text{-H})\text{-}(H_2CO)]^-$ abundance, which is maintained constant.

On the other hand, additional results provided from the experimental labeling are consistent with the consecutive [H_2+ C_2H_4] releases. Indeed, CID spectra of both the labeled $[\mathbf{III}_{\boldsymbol{\alpha}}\text{,d3-D}]^-$ and $[\mathbf{III}_{\boldsymbol{\beta}}\text{,d3-D}]^-$ precursor ions display the specific loss of the formal C_2H_5D neutral. This specificity can be explained by the consecutive losses of HD + C_2H_4 occurring via formation of the $[(M_{d3}\text{-D})\text{-HD}]^-$ ion specifically produced (see supplementary material, S2). This behavior differs significantly from that of the formaldehyde loss, since H_2CO and HDCO are competitively lost with relative intensity depending on the α/β stereochemistry. This loss of specific labeling is consistent with the DR experiments.

Another possibility must be considered that concerns the competitive CO and C_2H_4 losses as a first step prior to the H_2 loss. This consecutive process can be evidenced (or ruled out) from the DR experiments on the non-resolved *m/z* 259 (i.e., mixture of the isobaric *m/z* 259.1705 and 259.1340 product ions of $[M - H]^-$ due to the losses of CO and C_2H_4, respectively. The ejection of both isobaric ions was performed carefully to avoid direct *m/z* 257 ion ejection, which could yield ambiguities. By controlling the DR amplitude, it was possible to eject specifically the *m/z* 259 ion. The consecutive loss of

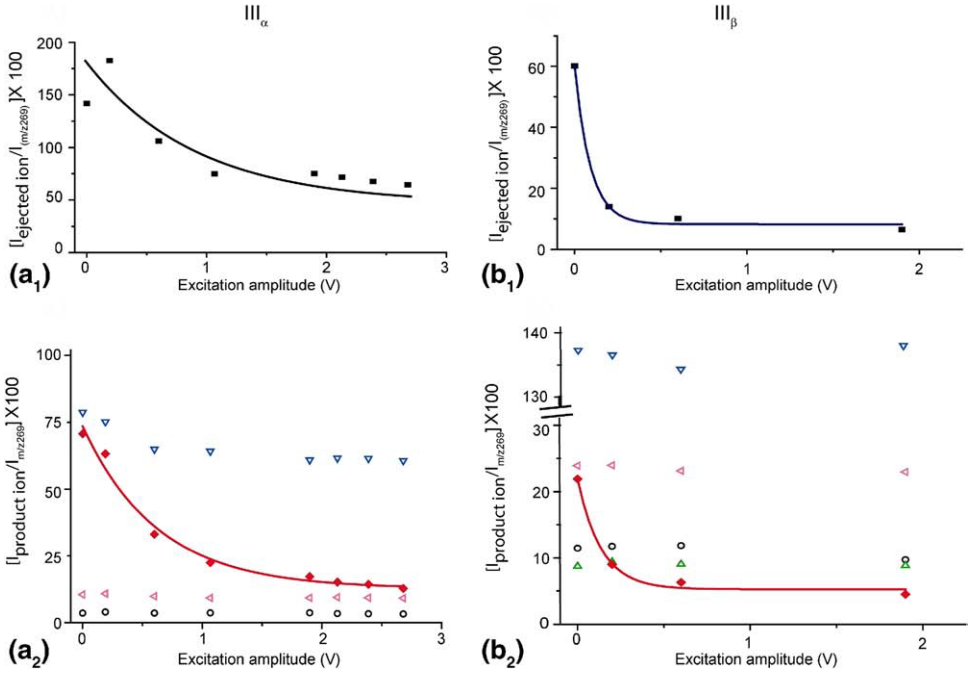

Figure 3. Abundance evolutions (**a**) of the isobaric [(**III**$_\alpha$-H)-30]$^-$ product ions by amplitude variation of the selected frequency applied for the controlled ejection of the *m/z* 285 product ion (prepared by IRMPD activation of the [**III**$_\alpha$-H]$^-$ precursor ion), and (**b**) of the isobaric [(**III**$_\beta$-H)-30]$^-$ product ions; [(filled square) *m/z* 285, (open circle) *m/z* 259 (−CO), (open triangle) *m/z* 259 (−C_2H_4), (inverted open triangle) *m/z* 257 (−H_2-CO), (filled diamond) *m/z* 257 (−H_2-C_2H_4), and (◁) *m/z* 241].

H_2 from the *m/z* 259 ion does not occur since the DR experiments applied to the *m/z* 259 ion do not result in partial or total *m/z* 257 ion abundance reduction.

All these results confirm that the CH_2O is lost through a one-step process in contrast to the C_2H_6 release, which takes place via losses of H_2 followed by consecutive loss of C_2H_4.

The formaldehyde release is not accompanied by large stereochemical effect since its abundance decreases from 2.8% to 1.5% for **III**$_\alpha$ and **III**$_\beta$, respectively (Table 3). However, the dissociation of the [**III**$_{\alpha,d3}$-D]$^-$ and [**III**$_{\beta,d3}$-D]$^-$ labeled precursor ions yields product ions at *m/z* 259 and 258 through the H_2CO and HDCO losses, respectively. For the α epimer, the H_2CO/HDCO ratio is 2:3 whereas for the β epimer the H_2CO/HDCO ratio is 4:1. If the H_2CO/HDCO loss variation can contribute to stereochemical effects, its rationalization is difficult without systematic CH labeling of the steroid skeleton. Thus, this loss will not be discussed further. Consequently, the interpretation will be focused on the (H_2 + C_2H_4) double-step losses, which present a spectacular specificity concerning the C_2H_5D loss from the labeled precursor ions. This release appears be due to the initial specific HD loss followed by C_2H_4 loss (a mechanism is proposed in supplementary material, S2). Interestingly, this release is not accompanied by that of C_2H_3D from a hypothetical H/D randomization. This suggests that in any case, H/D exchange can take place during the ethylene loss process from the [(M-H)-H_2]$^-$ alkoxide, which is described in Scheme 2.

These epimeric steroids decompose via competitive dissociations with rate constants depending upon the presence of the $C_{(11)}$ group and its stereochemistry, which allows to distinguish the 11α-OH-17β-estradiol (**III**$_\alpha$) and 11β-OH-17β-estradiol (**III**$_\beta$) without ambiguities. In view of these differences, one wonders if the gas-phase acidity of phenolic group is also influenced by the $C_{(11)}$ stereochemistry.

Gas-Phase Acidity of the Steroids

Deprotonated heterodimers, consisting of an analyte (A_0) and a reference compound (A_i) (Table 5), have been

Table 5. ΔH°_{acid} (kJ mol^{-1}) of the references

	M_w (u)	ΔH°_{acid}* (kJ mol^{-1})
(a) Carboxylic acids		
4-Pentenoic acid [70]	100	1441 ± 12
Cyclopentylacetic acid [71]	128	1446 ± 9.2
Valeric acid [71]	102	1449 ± 8.8
Butyric acid [71]	88	1450 ± 9.2
Propionic acid [71]	74	1454 ± 9.2
(b) Phenols		
para-F phenol [69]	112	1451 ± 8.8
meta-OMe phenol [69]	124	1456 ± 8.8
meta-CMe_3 phenol [69]	150	1459 ± 8.8
meta-Me phenol [69]	108	1463 ± 8.8

Used methods: ion/molecule reaction equilibrium [69, 71], collision induced dissociation and kinetic methods [70].
*From NIST webbook [68].

prepared with an electrospray ionization source from a 1:1 mixture of both species. For each gas-phase acidity measurement, the used A_i references should be structurally similar between them and have a known $\Delta H°_{acid}$ close to that of the analyte. Hence, the references used in this work are either carboxylic acids or substituted phenols (Table 5) [68–71]. This technique appears as a "handrail" because of the possibility to control life-time of the heterodimers through desolvation parameters. According to this statement, our experimental conditions (source condition, partner, concentrations, solvent composition, . . .) are optimized to get heterodimers with a good yield. For instance, the Figure 4a presents the ESI mass spectrum of a **I**/*para*-ethyl phenol mixture recorded under negative ion mode and weak declustering potential. Under these conditions, the deprotonated heterodimer $[A_0 + A_i\text{-}H]^-$ is observed at *m/z* 393. Under collision-induced dissociations, the $[A_0 + A_i\text{-}H]^-$ heterodimers yield the two $[A_0\text{-}H]^-$ and $[A_i\text{-}H]^-$ deprotonated molecules with relative abundances reflecting the respective gas-phase acidity of A_0 and A_i (Figure 4b). It is noteworthy that under soft desolvation conditions,

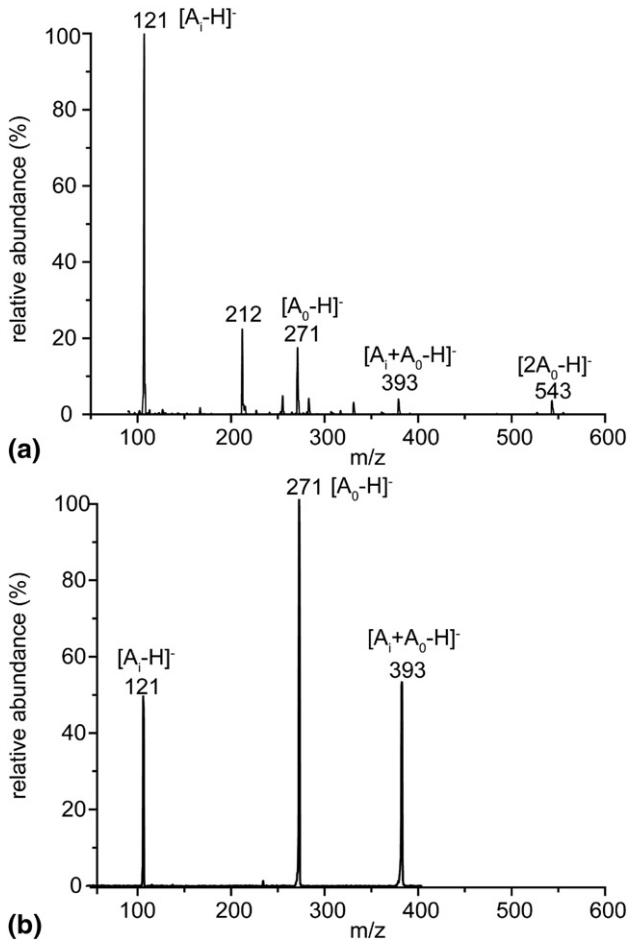

Figure 4. (**a**) ESI mass spectrum of **I** (A_0) and *para*-ethyl phenol (A_i) mixture. (**b**) CID spectrum of deprotonated heterodimer $[A_i+A_0\text{-}H]^-$, $E_{coll.}$ = 20 eV in collision cell of triple quadrupole.

the $[A_i\text{-}H]^-$ (Figure 4a) is produced as the base peak, whereas CID spectrum of $[A_0 + A_i\text{-}H]^-$, yields $[A_0\text{-}H]^-$ as the base peak. This result is not contradictory as the relative abundance in the ESI mass spectrum reflects numerous factors, such as solvation, solvent composition [72], and not only gas-phase acidity.

According to Cooks' method, data obtained from the competitive heterodimer dissociations allow to establish, for each collision energy, the plot $\ln(k_i/k_0)$ versus $\Delta H°_{acid}(A_i)$, and thus, $GA^{app}_{T_{eff}}(A_0, A_i)$ and T_{eff} values (Figures 5 and 6). The $\Delta H°_{acid}$ values are determined by the Armentrout's alternative treatment (Table 6). It should be stressed that consecutive decompositions are observed in certain cases. In particular, several carboxylic acid references yield a significant generation of secondary product ions corresponding to the loss of carbon dioxide from 4-pentenoic acid. So as not underestimate the relative abundance of these ions, the intensity of the consecutive product ions are added to that of the corresponding acidic monomer.

It is shown that gas-phase acidity values depend significantly on the substituent at $C_{(11)}$ position. It was found that the acidity order is: (**III**$_{\boldsymbol{\beta}}$) $\gg$ (**II**) $>$ (**I**) $>$ (**III**$_{\boldsymbol{\alpha}}$) (Table 6). It is noteworthy that errors in the $\Delta H°_{acid}(A_i)$ values are about $\pm$4 to $\pm$12 kJ mol^{-1} ($\pm$9 to $\pm$30 J mol^{-1} K^{-1} for activation entropy differences) [73]. The $\Delta\Delta S°(A_0, A_i)$ difference is large (more than 20 J mol^{-1} K^{-1}), and may yield relatively large systematic errors.

To confirm this experimental data, DFT calculations were carried out. Both experimental and theoretical results are consistent within the uncertainties (Table 6). It should be noted that for such a theoretical study, the structures considered are of fundamental importance as they can influence the results obtained. For this reason, it is necessary to built and to fully optimize numerous chemically relevant conformers for each compound. More precisely, structures characterized by different relative conformations of the cycles and $C_{(11)}$ hydroxyl group H-bond linkage have been considered. Theoretical calculations show that structures in which the nonaromatic six-membered ring is in a chair-like conformation are systematically the most stable ones. Optimizations have been carried out at the B3LYP/6-31G* level of theory for this study. Moreover, in the case of the estradiol derivates (**III**$_{\boldsymbol{\alpha}}$ and **III**$_{\boldsymbol{\beta}}$), three types of compounds could be formed, depending on the deprotonation site. A priori deprotonation can take place either on the phenol group or the hydroxyl group on the nonaromatic six-membered ring, or that of the five-membered ring. Our results confirm that the phenol group deprotonation is the less endothermic one. For example, Table 7 summarizes the energy of these three types of deprotonated structures for the most stable structures. The structures involving the deprotonation of the phenol group are systematically the most stable ones.

In this present work, the main factors that can influence the gas-phase acidity are polarity, dipole-dipole interaction, and charge-dipole interaction [74]. Herein, the influ-

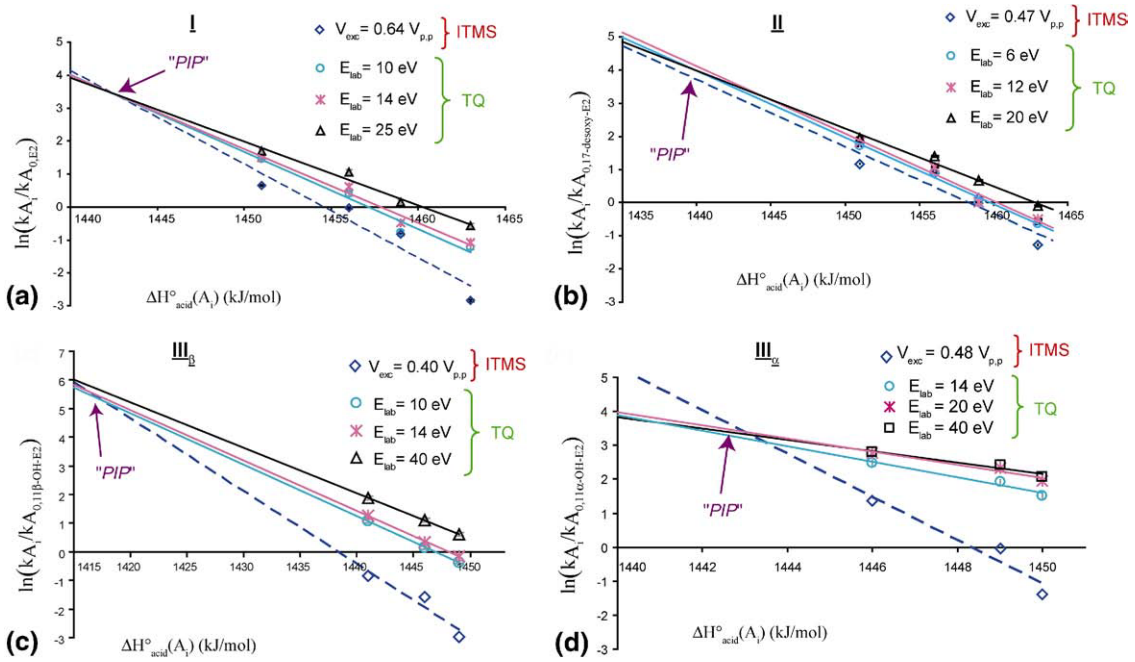

Figure 5. Plots $\ln(k_{Ai}/k_{A0})$ versus ΔH°_{acid} for (**a**) E_2, **I**, (**b**) 17-desoxy-E_2, **II**, (**c**) 11β-OH-17β-E_2, **III**$_{\beta}$, (**d**) 11α-OH-E_2, **III**$_{\alpha}$.

ence of the hydroxyl group on the gas-phase acidity is explored. The slight acidity difference between **I** and **II** suggests that the hydroxyl at $C_{(17)}$ does not influence significantly the phenol acidity. On the contrary, the values obtained for the **I** diol and the **III**$_{\beta}$ triol (hydroxyl addition at $C_{(11)}\beta$) are significantly different.

The fact that **I** and **II** present very close acidity suggests that the addition of one hydroxyl group does not influence significantly the polarity of the molecules. Indeed, an increase of the polarity should yield an increase of the gas-phase acidity through the stabilization of the corresponding anion. However, the addition of an hydroxyl group in $C_{(11)}$ position leads to a significant rise of gas-phase acidity, probably through charge–dipole interactions [75]. These results show that the charge–dipole interaction due to the substituent at $C_{(11)}$ have an important role in the modulation of the gas-phase acidity of steroids.

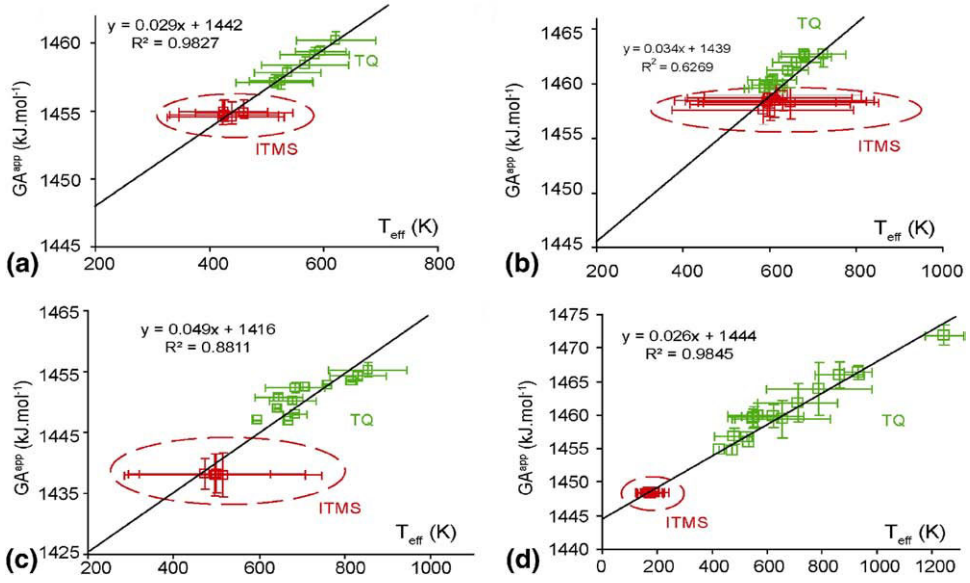

Figure 6. Plots GA^{app} versus T_{eff} for (**a**) E_2 **I**, (**b**) 17-desoxy-E_2 **II**, (**c**) 11β-OH-17β-E_2 **III**$_{\beta}$, (**d**) 11α-OH-E_2 **III**$_{\alpha}$. The data pairs GA^{app} and T_{eff} reported have been obtained by using both the ion trap (inside the circle in dotted line) and triple quadrupole instruments. (Linear extrapolation was used under the known method limitations).

Table 6. Experimental ΔH°_{acid} and $\Delta\Delta S^{\circ}$ (A_0, A_i) values of E_2 and its 11-substituted derivatives. Comparison with theoretical ΔH°_{acid} values

Compounds	$\Delta H^{\circ}_{acid}(A_0)_{exp}$[a] (kJ mol^{-1})	$D\Delta S^{\circ}(A_0, A_i)_{exp}$[a] (J mol^{-1} K^{-1})	$\Delta H^{\circ}_{acid}(A_0)_{calc}$[d] (kJ mol^{-1})
I[b]	1442 ± 10 (1)	−29 ± 20 (1)	1439
II[b]	1439 ± 10 (4)	−34 ± 20 (7)	1440
$\mathbf{III}_{\beta}$[c]	1416 ± 10 (3)	−49 ± 20 (5)	1419
$\mathbf{III}_{\alpha}$[c]	1444 ± 10 (1)	−26 ± 20 (1)	1449

[a] ΔH°_{acid} and $\Delta\Delta S^{\circ}(A_0, A_i)$ obtained using the Armentrout's alternative treatment.
[b] Substituted phenols were the used references.
[c] Carboxylic acids were the used references.
[d] Acidity values obtained by using DFT.

In addition, the experimental variation of acidity between both the $\mathbf{III}_{\beta}$ and $\mathbf{III}_{\alpha}$ stereoisomers is large, i.e., 28 kJ mol^{-1}, which is very similar to that obtained by DFT calculations ($\Delta\Delta H^{\circ}_{acid(calc)}$ = 30 kJ mol^{-1}). Thus, the hydroxyl group at $C_{(11)}\beta$ position seems to play a key role in the acidity of the steroid derivatives whereas no significant effect appears when hydroxyl is at the $C_{(11)}\alpha$ position. Hence, these data indicate that in addition to the charge–dipole interaction, other structural parameters have a significant role in the modulation of the gas-phase acidity of steroids. To explain why the $\mathbf{III}_{\beta}$ is more acidic than $\mathbf{III}_{\alpha}$, a mechanism involving stereospecific proton interaction with the A ring has been proposed (Scheme 4) [71].

In this section, we intend to explain the role of this $C_{(11)}$ hydroxyl group on the gas-phase acidity of steroids. A priori, various groups such as phenol or secondary aliphatic hydroxyl could be deprotonated. The gas-phase acidity values of mono-substituted phenols are in the 1370–1480 kJ mol^{-1} range, whereas for cyclohexanediol it is in the 1474–1520 kJ mol^{-1} range [68, 76]. This indicates that in our case the measured acidities are those of the phenol hydroxyl site. Surprisingly, the stereochemical effect at $C_{(11)}$ is important, as apparently the β isomer presents an acidity significantly higher than that of the α isomer. These results agree with the literature since it has been shown that in the case of cyclohexanol compounds, the β hydroxyl group is more acidic than the α [36, 76]. This class of stereoisomer with *cis* and *trans* disubstituted ring has a great interest to rationalize the influence of the stereochemistry. For example, in the case of isomeric *cis* and *trans* 1,4-cyclohexanediols, the stereochemical effects on relative acidity were interpreted as a result of hydrogen-bond stabilization that occurs in the case of *cis* isomer [37]. Brauman et al. proposed the same interpretation in another study [76]. Moreover, Cooks and his coworkers have shown that the acidity differences between several 2-3-butanediol stereoisomers are caused by steric repulsion [35].

The stereochemistry effect in our case can be explained by considering that the hydroxyl proton at $C_{(11)}$ is involved in an interaction with the aromatic ring yielding an increase of the phenol acidity (Scheme 4). The axial proton at $C_{(11)}$ interaction with the aromatic group is favored for $[\mathbf{III}_{\beta}\text{-H}]^-$ because of its position. This is in agreement with the proposed mechanisms presented previously to rationalize the stereochemical effects on the CID spectra (Scheme 2). Indeed, this interaction is easier for the $[\mathbf{III}_{\beta}\text{-H}]^-$ because the proton is above the π-orbital cloud of the aromatic ring, whereas for $[\mathbf{III}_{\alpha}\text{-H}]^-$ the proton is on the aromatic A ring and not in the π-orbital cloud (Scheme 4). The most stable conformations obtained from theoretical calculation shows that the distance between the H of $HO_{(11)}$ group and the $C_{(10)}$ is 2.7 Å for $[\mathbf{III}_{\alpha}\text{-H}]^-$ and 2.3 Å for $[\mathbf{III}_{\beta}\text{-H}]^-$. The lower distance for the $[\mathbf{III}_{\beta}\text{-H}]^-$ epimer is consistent with its higher acidity and with the previous hypothesis. In addition, it should be noted that the electron density calculated at $C_{(3)}$ seems to confirm this view since it is weaker for $[\mathbf{III}_{\beta}\text{-H}]^-$ (δ^+ = 0.39) than for $[\mathbf{III}_{\alpha}\text{-H}]^-$ (δ^+ = 0.23). Moreover, an electrostatic interaction involving the methyl group at $C_{(13)}$ and the oxygen atom at $C_{(11)}$ could take place when the hydroxyl group is in the axial orientation ($[\mathbf{III}_{\beta}\text{-H}]^-$). This interaction is reinforced by the steric repulsion occur-

Table 7. Influence of the deprotonation site on the relative stability of the compounds

	Deprotonation on the phenol group		Deprotonation on the non-aromatic six-ring cycle		Deprotonation on the five-ring cycle	
Name of neutral compound	Energy (Hartree)	ΔE (kJ mol^{-1})	Energy (Hartree)	ΔE (kJ mol^{-1})	Energy (Hartree)	ΔE (kJ mol^{-1})
$\mathbf{III}_{\alpha}$	−927.93743	0	−927.91109	69.2	−927.91154	68.0
$\mathbf{III}_{\beta}$	−927.94698	0.0	−927.90824	101.7	−927.90636	106.6

$\Delta E = E_{considered\ structure} - E_{of\ the\ most\ stable\ structure}$.

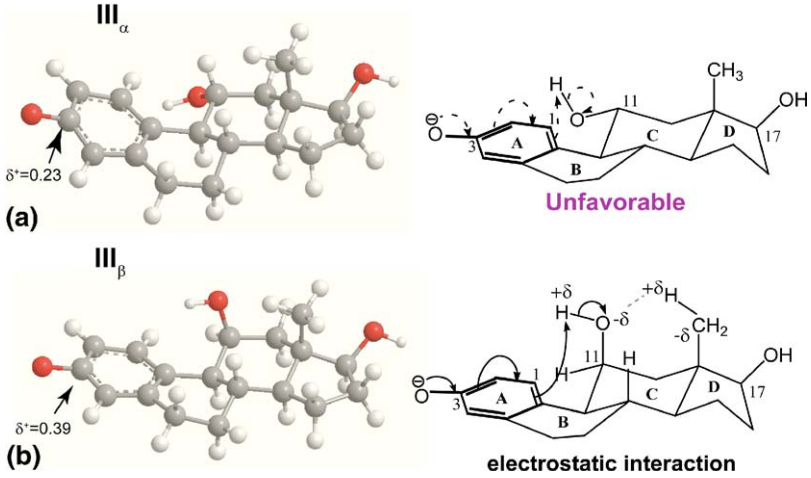

Scheme 4. Stereospecific proton transfer mechanism occurring in gas-phase conditions. (The atomic populations were calculated at the B3P86/6-31+G* level).

ring between the $C_{(18)}$ methyl and the oxygen at $C_{(17)}$. This effect results in stabilization of the $[\mathbf{III}_{\boldsymbol{\beta}}\text{-H}]^-$ anion. Hence, the $[\mathbf{III}_{\boldsymbol{\beta}}\text{-H}]^-$ epimer is more stable than the $[\mathbf{III}_{\boldsymbol{\alpha}}\text{-H}]^-$ epimer and, as a consequence, $\mathbf{III}_{\boldsymbol{\beta}}$ is more acidic than $\mathbf{III}_{\boldsymbol{\alpha}}$ because the $\Delta H°_f$ of neutrals were similar within the incertitude.

The present study reveals that the extended kinetic method is particularly well adapted to explore the intrinsic electronic changes induced by the presence of substituents at the $C_{(11)}$ position of estradiol derivatives and its stereochemistry. The stereochemistry effect could change the acidity of the analytes especially via stereospecific proton interaction with the π-orbital cloud of A ring. Hence, this work suggests that substituent-induced intramolecular electronic perturbations occur in estrogenic steroids and may consequently change the acidity of the phenolic hydroxyl (see Supplemental data, which can be found in the electronic version of this article).

Conclusion

In the context of stereochemical studies, the ERMS curves have shown that the steroids decompose by different pathways involving competitive dissociation reactions with rate constants depending upon the α/β $C_{(11)}$ stereochemistry. It was shown that the 11α-OH-17β-estradiol, $\mathbf{III}_{\boldsymbol{\alpha}}$, and 11$\beta$-OH-17$\beta$-estradiol, $\mathbf{III}_{\boldsymbol{\beta}}$, can be distinguished without ambiguities through the relative abundance differences of their product ion spectra especially through the *m/z* 285, 269, 259, and 257 ions corresponding to the losses of H_2, H_2O, ethylene and ethane, respectively. On the other hand, the H/D exchange experiments and double resonant experiments demonstrated that the α or β stereochemistry at $C_{(11)}$ orients strongly the fragmentation pathways although the initial deprotonation takes place regioselectively on the acidic phenolic site. When the hydroxyl group is at $C_{(11)}\beta$ position, the proton transfer from $C_{(11)}\beta$ hydroxyl group to the $C_{(10)}$ position is favored whereas this mechanism is strongly hindered when the hydroxyl is in the $C_{(11)}\alpha$ position.

The extended kinetic method was revealed to be particularly well adapted to explore the intrinsic electronic changes induced by the presence of substituents at the position $C_{(11)}$ of substituted estradiols. More precisely, the gas-phase acidity of phenolic hydroxyl changes in function of the stereochemistry at $C_{(11)}$ position. The stereochemical effects could change the acidity of the analytes, especially via stereospecific proton interaction with π-orbital cloud of A ring. Hence, this work suggests that the acidity of steroids could be modulated essentially by substituent-induced intramolecular electronic perturbations and not by polarity. These results have been confirmed using theoretical calculation.

The study of a larger series of estrogens substituted in $C_{(11)}$ is required to validate the effect of the substituent nature on the 3-hydroxyl gas-phase acidity and compare these values with the binding affinity values obtained in solution. This work showed that substituent-induced intramolecular electronic perturbations occur in estrogenic steroids and may consequently change the gas-phase acidity of the phenolic hydroxyl. This suggests that the anchoring strength with Glu-353 and Arg-394 of ERα and, therefore, the binding affinity of the ligands for ERα may be modulated by this way. This concept should be further considered in quantitative structure activity relationship (QSAR) studies and could constitute a new basis to elaborate ERα ligands.

Acknowledgments

The authors gratefully acknowledge financial supports from the French ministry of research, CNRS and UPMC. The authors sincerely appreciate Professor Peter B. Armentrout for giving them his program and for helpful discussion.

Appendix A
Supplementary Material

Supplementary material associated with this article may be found in the online version at doi:10.1016/j.jasms.2009.08.017.

References

1. Rapuri, J. P. B.; Gallagher, C.; Haynatzki, G. Endogenous Levels of Serum Estradiol and Sex Hormone Binding Globulin Determine Bone Mineral Density, Bone Remodeling, the Rate of Bone Loss, and Response to Treatment with Estrogen in Rlderly Women. *J. Clin. Endocrinol. Metab.* **2004,** *89*, 4954–4962.
2. Mendelsohn, M. E. Mechanisms of Estrogen Action in the Cardiovascular System. *J. Steroid Biochem. Mol. Biol.* **2000,** *74*, 337–343.
3. Garcia-Segura, L. M.; Azcoitia, I.; DonCarlos, L. L. Neuroprotection by Estradiol. *Prog. Neurobiol.* **2001,** *63*, 29–60.
4. Tsai, M. J.; O'Malley, B. W. Molecular Mechanisms of Action of Steroid/Thyroid Receptor Superfamily Members. *Annu. Rev. Biochem.* **1994,** *63*, 451–486.
5. Blair, R. M.; Fang, H.; Branham, W. S.; Hass, B. S.; Dial, S. L.; Moland, C. L.; Tong, W.; Shi, L.; Perkins, R.; Sheehan, D. M. The Estrogen Receptor Relative Binding Affinities of 188 Natural and Xenochemicals: Structural Diversity of Ligands. *Toxicol. Sci.* **2000,** *54*, 138–153.
6. Shi, L. M.; Fang, H.; Tong, W.; Wu, J.; Perkins, R.; Blair, R. M.; Branham, W. S.; Dial, S. L.; Moland, C. L.; Sheehan, D. M. QSAR Models Using a Large Diverse Set of Estrogens. *J. Chem. Inf. Comput. Sci.* **2001,** *41*, 186–195.
7. Anstead, G. M.; Carlson, K. E.; Katzenellenbogen, J. A. The Estradiol Pharmacophore: Ligand Structure–Estrogen Receptor Binding Affinity Relationships and a Model for the Receptor binding Site. *Steroids* **1997,** *62*, 268–303.
8. Brzozowski, A. M.; Pike, A. C.; Dauter, Z.; Hubbard, R. E.; Bonn, T.; Engstrom, O.; Ohman, L.; Greene, G. L.; Gustafsson, J. A.; Carlquist, M. Molecular Basis of Agonism and Antagonism in the Estrogen Receptor. *Nature* **1997,** *389*, 753–758.
9. Shi, Y.; Koh, J. T. Selective Regulation of Gene Expression by an Orthogonal Estrogen Receptor–Ligand Pair Created by Polar-Group Exchange. *Chem. Biol.* **2001,** *8*, 501–510.
10. Bourgoin-Voillard, S.; Gallo, D.; Laïos, I.; Cleeren, A.; El Bali, L.; Jacquot, Y.; Nonclercq, D.; Laurent, G.; Tabet, J. C.; Leclercq, G. Capacity of Types I and II Ligands to Confer to Estrogen Receptor α an Appropriate Conformation for the Recruitment of Coactivators Containing a LxxLL Motif—Relationship with the Regulation of Receptor Level and ERE-Dependent Transcriptions in MCF-7 Cells. *Biochem. Pharmacol*., submitted.
11. Wiese, T. E.; Polin, L. A.; Palomino, E.; Brooks, S. C. Induction of the Estrogen Specific Mitogenic Response of MCF-7 Cells by Selected Analogs of Estradiol-17β: A 3D QSAR Study. *J. Med. Chem.* **1997,** *40*, 3659–3669.
12. Lobaccaro, C.; Pons, J. F.; Duchesne, M. J.; Auzou, G.; Pons, M.; Nique, F.; Teutsch, G.; Borgna, J. L. Steroidal Affinity Labels of the Estrogen Receptor α. 3. Estradiol 11β-n-alkyl Derivatives Bearing a Terminal Electrophilic Group: Antiestrogenic and Cytotoxic Properties. *J. Med. Chem.* **1997,** *40*, 2217–2227.
13. Aliau, S.; Delettre, G.; Mattras, H.; El Garrouj, D.; Nique, F.; Teutsch, G.; Borgna, J. L. Steroidal Affinity Labels of the Estrogen Receptor α. 4. Electrophilic 11β-Aryl Derivatives of Estradiol. *J. Med. Chem.* **2000,** *43*, 613–628.
14. Voillard, S.; Zins, E. L.; Fournier, F.; Jacquot, Y.; Afonso, C.; Pèpe, C.; Leclercq, G.; Tabet, J. C. Stereochemical Effects of Substituents in Position 11 of 17-β-Estradiol on Gas Phase Acidity: A Cooperative Effect. *Proceedings of the 56th ASMS Conference on Mass Spectrometry*, Denver, CO, June, 2008; 19(Suppl 1), S57–S84.
15. Splitter, J. S.; Turecek, F. *Applications of Mass Spectrometry to Organic Stereochemistry*; VCH: New York, 1994; p. 705.
16. Mandelbaum, A. Stereochemical effects in mass spectrometry. *Adv. Mass Spectrom.* **1995,** *13*, 227–240.
17. Meyerson, S.; Weitkamp, A. W. Stereoisomeric Effects on Mass Spectra. I. *Org. Mass Spectrom.* **1968,** *1*, 659–667.
18. Green, M. M. Mass Spectrometry and the Stereochemistry of Organic Molecules. *Topics Stereochem.* **1976,** *9*, 35–110.
19. Mandelbaum, A. Stereochemical Effects in Mass Spectrometry. *Mass Spectrom. Rev.* **1983,** *2*, 223–284.
20. Turecek, F. Stereochemistry of Organic Ions in the Gas Phase: A review. *Collect. Czech. Chem. Commun.* General Review. **1987,** *52*, 1928–1984.
21. Richter, W. J.; Schwarz, H. Chemical Ionization—A Highly Important Productive Mass Spectrometric Analysis Method. *Angew. Chem. Int. Ed.* **1978,** *90*, 449–469.
22. Tabet, J. C.; Hanna, I.; Fetizon, M. Stereospecific Hydride Transfer Under NCI/Hydroxide Ion Conditions. 2. Origins of the C_2H_4O Elimination from Stereoisomeric Alkoxyketal Derivatives. *Org. Mass Spectrom.* **1985,** *20*, 61–64.
23. Tabet, J. C. Ion–Molecule Reactions and Stereochemistry in Tandem Mass Spectrometry. *NATO ASI Ser. Ser. C* **1991,** *347*, 351–372.
24. Winkler, F. J.; Stahl, D. Stereochemical Effects on Anion Mass Spectra of Cyclic Diols. Negative Chemical Ionization, Collisional Activation, and Metastable Ion Spectra. *J. Am. Chem. Soc.* **1978,** *100*, 6779–6780.
25. Houriet, R.; Stahl, D.; Winkler, F. J. Negative Chemical Ionization of Alcohols. *Environ. Health Perspect.* **1980,** *36*, 63–68.
26. Beloeil, J. C.; Bertranne, M.; Stahl, D.; Tabet, J. C. Stereochemistry of Gaseous Anions: Hydroxide Ion Negative Chemical Ionization of 17-ζ-R-5α, 14β-Androstane-14, 17ζ-Diols. *J. Am. Chem. Soc.* **1983,** *105*, 1355–1359.
27. Dreyer, U.; Suelzle, D.; Schroeder, D.; Schwarz, H. Kinetic Isotope Effects and exo/endo-Face Selectivity in the Unimolecular Dehydrogenation of Norborneol Alkoxides in the Gas Phase. *Helv. Chim. Acta* **1990,** *73*, 2179–2182.
28. Minamisawa, T.; Hirabayashi, J. Fragmentations of Isomeric Sulfated Monosaccharides Using Electrospray Ion Trap Mass Spectrometry. *Rapid Commun. Mass Spectrom.* **2005,** *19*, 1788–1796.
29. Fang, T. T.; Bendiak, B. The Stereochemical Dependence of Unimolecular Dissociation of Monosaccharide-Glycolaldehyde Anions in the Gas Phase: A. Basis for Assignment of the Stereochemistry and Anomeric Configuration of Monosaccharides in Oligosaccharides by Mass Spectrometry via a Key Discriminatory Product Ion of Disaccharide Fragmentation, *m/z* 221. *J. Am. Chem. Soc.* **2007,** *129*, 9721–9736.
30. Splitter, J. S.; Turecek, F.; Tabet, J. C. *Applications of Mass Spectrometry to Organic Stereochemistry*; VCH: New York, 1994; Chap. XIX, pp 543–623.
31. Fournier, F.; Tabet, J. C.; Debrauwer, L.; Rao, D.; Paris, A.; Bories, G. Structural Dependence of Anion/Dipole Complex Upon the Deprotonated Site in $[M - H]^-$ Ions of 17β-Estradiol-17-Stearate Ester in Ammonia Negative-Ion Chemical Ionization. *Rapid Commun. Mass Spectrom.* **1991,** *5*, 44–47.
32. Cooks, R. G.; Kruger, T. L. Intrinsic Basicity Determination Using Metastable Ions. *J. Am. Chem. Soc.* **1977,** *99*, 1279–1281.
33. Wright, L. G.; McLuckey, S. A.; Cooks, R. G.; Wood, K. V. Relative Gas-Phase Acidities from Triple Quadrupole Mass Spectrometers. *Int. J. Mass Spectrom. Ion Phys.* **1982,** *42*, 115–124.
34. Cheng, X.; Wu, Z.; Fenselau, C. Collision Energy Dependence of Proton-Bound Dimer Dissociation: Entropy Effects, Proton Affinities, and Intramolecular Hydrogen-Bonding in Protonated Peptides. *J. Am. Chem. Soc.* **1993,** *115*, 4844–4848.
35. Shen, W.; Wong, P. S. H.; Cooks, R. G. Stereoisomeric Distinction by the Kinetic Method: 2,3-Butanediol. *Rapid Commun. Mass Spectrom.* **1997,** *11*, 71–74.
36. Majumdar, T. K.; Clairet, F.; Tabet, J. C.; Cooks, R. G. Epimer Distinction and Structural Effects on Gas-Phase Acidities of Alcohols Measured Using the Kinetic Method. *J. Am. Chem. Soc.* **1992,** *114*, 2897–2903.
37. Houriet, R.; Tabet, J. C.; Tchapla, A. Gas-Phase Acidity of Aliphatic and Cyclic Diols. *Spectroscopy* (Amsterdam, The Netherlands) **1984,** *3*, 132–138.
38. Chen, X.; Walthall, D. A.; Brauman, J. I. Acidities in Cyclohexanediols Enhanced by Intramolecular Hydrogen Bonds. *J. Am. Chem. Soc.* **2004,** *126*, 12614–12620.
39. Haas, M. J.; Harrison, A. G. The Fragmentation of Proton-Bound Cluster Ions and the Gas-Phase Acidities of Alcohols. *Int. J. Mass Spectrom. Ion Processes* **1993,** *124*, 115–124.
40. Bartmess, J. E.; Scott, J. A.; McIver, R. T., Jr. Scale of Acidities in the Gas Phase from Methanol to Phenol. *J. Am. Chem. Soc.* **1979,** *101*, 6046–6056.
41. Armentrout, P. B. Entropy Measurements and the Kinetic Method: A Statistically Meaningful Approach. *J. Am. Soc. Mass Spectrom.* **2000,** *11*, 371–379.
42. Vekey, K. Internal Energy Effects in Mass Spectrometry. *J. Mass Spectrom.* **1996,** *31*, 445–463.
43. Drahos, L.; Vekey, K. How Closely Related are the Effective and the Real Temperature? *J. Mass Spectrom.* **1999,** *34*, 79–84.
44. Ervin, K. M. Microcanonical Analysis of the Kinetic Method. The Meaning of the "Effective Temperature." *Int. J. Mass Spectrom.* **2000,** *195/196*, 271–284.
45. Nold, M. J.; Cerda, B. A.; Wesdemiotis, C. Proton Affinities of the N- and C-Terminal Segments Arising Upon the Dissociation of the Amide Bond in Protonated Peptides. *J. Am. Soc. Mass Spectrom.* **1999,** *10*, 1–8.
46. Drahos, L.; Vekey, K. Entropy Evaluation Using the Kinetic Method: Is it Feasible? *J. Mass Spectrom.* **2003,** *38*, 1025–1042.
47. Mezzache, S.; Bruneleau, N.; Vekey, K.; Afonso, C.; Karoyan, P.; Fournier, F.; Tabet, J. C. Improved Proton Affinity Measurements for Proline and Modified Prolines Using Triple Quadrupole and Ion Trap Mass Spectrometers. *J. Mass Spectrom.* **2005,** *40*, 1300–1308.
48. Drahos, L.; Peltz, C.; Vekey, K. Accuracy of Enthalpy and Entropy Determination Using the Kinetic Method: Are We Approaching a Consensus? *J. Mass Spectrom.* **2004,** *39*, 1016–1024.
49. March, R. E. An Introduction to Quadrupole Ion Trap Mass Spectrometry. *J. Mass Spectrom.* **1997,** *32*, 351–369.
50. Frisch, M. J.; Trucks, G. W.; Schlegel, H. B.; Scuseria, G. E.; Robb, M. A.; Cheeseman, J. R.; Zakrzewski, V. G.; Montgomery, J. A.; Stratmann, R. E.; Jr.; Burant, J. C.; Dapprich, S.; Millam, J. M.; Daniels, A. D.; Kudin, K. N.; Strain, M. C.; Farkas, O.; Tomasi, J.; Barone, V.; Cossi, M.; Cammi, R.; Mennucci, B.; Pomelli, C.; Adamo, C.; Clifford, S.; Ochterski, J.; Petersson, G. A.; Ayala, P. Y.; Cui, Q.; Morokuma, K.; Rega, N.; Salvador, P.; Dannenberg, J. J.; Malick, D. K.; Rabuck, A. D.; Raghavachari, K.; Foresman, J. B.; Cioslowski, J.; Ortiz, J. V.; Baboul, A. G.; Stefanov, B. B.; Liu, G.; Liashenko, A.; Piskorz, P.; Komaromi, I.;

Gomperts, R.; Martin, R. L.; Fox, D. J.; Keith, T.; Al-Laham, M. A.; Peng, C.Y.; Nanayakkara, A.; Challacombe, M.; Gill, P. M. W.; Johnson, B.; Chen, W.; Wong, M. W.; Andres, J. L.; Gonzalez, C.; Head-Gordon, M.; Replogle, E.S.; Pople, J. A. *Gaussian 03*; Gaussian, Inc.: Pittsburgh PA, 2002.

51. Becke, A. D. Density-Functional Exchange-Energy Approximation with Correct Asymptotic Behavior. *Phys. Rev. A.* **1988,** *38*, 3098–3100.
52. Perdew, J. P. Density-Functional Approximation for the Correlation Energy of the Inhomogeneous Electron Gas. *Phys. Rev. B* **1986,** *33*, 8822–8824.
53. Perdew, J. P. Erratum: Density-Functional Approximation for the Correlation Energy of the Inhomogeneous Electron Gas. *Phys. Rev. B.* **1986,** *34*, 7406–7406.
54. Brandan, S. A. Theoretical Study of the Structure and Vibrational Spectra of Chromyl Perchlorate, $CrO_2(ClO_4)_2$. *Theochem.* **2009,** *908*, 19–25.
55. Zhidomirov, G. M.; Larin, A. V.; Trubnikov, D. N.; Vercauteren, D. P. Ion-Exchanged Binuclear Clusters as Active Sites of Selective Oxidation over Zeolites. *J. Phys. Chem. C* **2009,** *113*, 8258–8265.
56. Rochut, S.; Pepe, C.; Paumard J. P.; Tabet J. C. A Computational and Experimental Study of Cation Affinity (Na+) of Nucleobases and Modified Nucleobases by Electrospray Ionization Ion Trap Mass Spectrometry. *Rapid Commun. Mass Spectrom.* **2004,** *18*, 1686–1692.
57. Pepe, C.; Rochut, S.; Paumard, J. P.; Tabet, J. C. Ab Initio Calculations of Proton Affinities of Glycine, Proline, Cysteine, and Phenylalanine: Comparison with the Experimental Values Obtained Using an Electrospray Ionization Ion Trap Mass Spectrometer. *Rapid Commun. Mass Spectrom.* **2004,** *18*, 307–312.
58. Hua, Y.; Cole, R. B. Electrospray Ionization Tandem Mass Spectrometry for Structural Elucidation of Protonated Brevetoxins in Red Tide Algae. *Anal. Chem.* **2000,** *72*, 376–383.
59. Beland, F. A.; Churchwell, M. I.; Von Tungeln, L. S.; Chen, S.; Fu, P. P.; Culp, S. J.; Schoket, B.; Gyrffy, E.; Minrovits, J.; Poirier, M. C.; Bowman, E. D.; Weston, A.; Doerge, D. R. High-Performance Liquid Chromatography Electrospray Ionization Tandem Mass Spectrometry for the Detection and Quantitation of Benzo[α]Pyrene-DNA Adducts. *Chem. Res. Toxicol.* **2005,** *18*, 1306–1315.
60. Daikoku, S.; Ako, T.; Kato, R.; Ohtsuka, I.; Kanie, O. Discrimination of 16 Structural Isomers of Fucosyl Galactoside Based on Energy-Resolved Mass Spectrometry. *J. Am. Soc. Mass Spectrom.* **2007,** *18*, 1873–1879.
61. Laskin, J.; Bailey, T. H.; Futrell, J. H. Fragmentation Energetics for Angiotensin II and Its Analogs from Time- and Energy-Resolved Surface-Induced Dissociation Studies. *Int. J. Mass Spectrom.* **2004,** *234*, 89–99.
62. Ho, Y.; Kebarle, P. Studies of the Dissociation Mechanisms of Deprotonated Mononucleotides by Energy Resolved Collision-Induced Dissociation. *Int. J. Mass Spectrom. Ion Processes* **1997,** *165/166*, 433–455.
63. Kumar, M. R.; Prabhakar, S.; Reddy, T. J.; Vairamani, M. Generation of Alkoxide Anions from a Series of Aliphatic Diols and Alcohols and Their Ion–Molecule Reactions with Carbon Dioxide in the Gas Phase. *Eur. J. Mass Spectrom.* **2006,** *12*, 19–24.
64. Gaeumann, T.; Stahl, D.; Tabet, J. C. The Mechanism of the Loss of Hydrogen and Water from 1,4-Cyclohexanediol Anion and Related Compounds. *Org. Mass Spectrom.* **1983,** *18*, 263–267.
65. Decouzon, M.; Gal, J. F.; Geribaldi, S.; Rouillard, M.; Sturla, J. M. Differentiation of Diastereoisomeric Terpenoid Alcohols by Electron Impact and Negative Ion Chemical Ionization Associated with Collision-Induced Dissociation. A Fourier Transform Ion Cyclotron Resonance Study. *Org. Mass Spectrom.* **1990,** *25*, 312–316.
66. Decouzon, M.; Geribaldi, S. Negative-Ion Chemical Ionization-Collision-Induced Dissociation Study of Unsubstituted Cycloalkanols, Alkanones, and Alkenones at Low Collisional Energy. *Rapid Commun. Mass Spectrom.* **1992,** *6*, 140–142.
67. Winkler, F. J.; Stahl, D. Stereochemical Effects on Anion Mass Spectra of Cyclic Diols. Negative Chemical Ionization, Collisional Activation, and Metastable Ion Spectra. *J. Am. Chem. Soc.* **1978,** *100*, 6779–6780.
68. Linstrom, P. J.; Mallard, W. G. Eds. NIST Chemistry WebBook, NIST Standard Reference Database Number 69, National Institute of Standards and Technology, Gaithersburg MD, 20899, http://webbook.nist.gov.
69. Fujio, M.; McIver, R. T., Jr.; Taft, R. W. Effects of the Acidities of Phenols from Specific Substituent–Solvent Interactions. Inherent Substituent Parameters from Gas-Phase Acidities. *J. Am. Chem. Soc.* **1981,** *103*, 4017–4029.
70. Graul, S. T.; Schnute, M. E.; Squires, R. R. Gas-Phase Acidities of Carboxylic Acids and Alcohols from Collision-Induced Dissociation of Dimer Cluster Ions. *Int. J. Mass Spectrom. Ion Processes* **1990,** *96*, 181–198.
71. Caldwell, G. W.; Renneboog, R.; Kebarle, P. Gas-Phase Acidities of Aliphatic Carboxylic Acids, Based on Measurements of Proton-Transfer Equilibria. *Can. J. Chem.* **1989,** *67*, 611–618.
72. Cole, R. B.; Harrata, A. K. Solvent Effect on Analyte Charge State, Signal Intensity, and Stability in Negative Ion Electrospray Mass Spectrometry; Implications for the Mechanism of Negative Ion Formation. *J. Am. Soc. Mass Spectrom.* **1993,** *4*, 546–556.
73. Ervin, K. M.; Armentrout, P. B. Systematic and Random Errors in Ion Affinities and Activation Entropies from the Extended Kinetic Method. *J. Mass Spectrom.* **2004,** *39*, 1004–1015.
74. Brauman, J. I.; Blair, L. K. Gas-Phase Acidities of Alcohols. Effects of Alkyl Groups. *J. Am. Chem. Soc.* **1968,** *90*, 6561–6562.
75. Walthall, D. A.; Brauman, J. I. Vinyl Hydrogen Acidities of Two Stereoisomers. *J. Phys. Chem. A* **2007,** *111*, 1362–1367.
76. Chen, X.; Walthall, D. A.; Brauman, J. I. Acidities in Cyclohexanediols Enhanced by Intramolecular Hydrogen Bonds. *J. Am. Chem. Soc.* **2004,** *126*, 12614–12620.